MM Science Journal | www.mmscience.eu
ISSN 1803-1269 (Print) | ISSN 1805-0476 (On-line)
Special Issue | HSM 2025
18th International Conference on High Speed Machining
October 15-16, 2025, Metz, France
DOI: 10.17973/MMSJ.2025_11_2025139

HSM2025-45013

TOOL WEAR INVESTIGATION OF COATED CEMENTED CARBIDE INSERTS DURING INTERRUPTED TURNING OF NODULAR CAST IRON

D. Andersson[1]*, A. Malakizadi[1]

[1]Chalmers University of Technology, Department of Industrial and Materials Science, Gothenburg, Sweden

*Corresponding author; e-mail: daniel.j.andersson@chalmers.se

Abstract
This study investigates the wear mechanisms for two different cemented carbide grades during intermittent turning of nodular cast iron. Turning tests with in-situ force measurements were performed on workpieces with axially oriented grooves. An in-depth analysis of tools and the workpiece material was conducted utilising scanning electron microscopy (SEM) and energy-dispersive X-ray spectroscopy (EDS). Based on the material characterisation, the workpiece material was found to contain a significant amount of abrasive non-metallic inclusions, typically triggering wear by abrasion and thus limiting the tool-life. The results show industrially applicable performance for both tested grades.

Keywords:
Turning, Tool wear, Nodular Cast Iron

1 INTRODUCTION

Cast irons are a group of materials widely utilised in several industries due to their ease of manufacturing, low cost, and good material performance [Górny, 2015]. An industry heavily reliant on cast irons is automotive manufacturing. Engine blocks and cylinder heads, as well as hubs and axles often rely on casting to achieve complex geometries without extensive machining. With higher demands on engine efficiency, as well as different requirements for electric powertrain components, much effort has been put towards increasing the material performance of cast irons. Commonly, this has entailed modifying the morphology of the graphite, either into spheroidal/nodular (SGI/NGI) or vermicular (CGI) morphologies as opposed to the flaky graphite found in conventional grey cast iron (GCI). These changes can improve the performance of cast iron, predominantly in terms of increased ductility. In the context of the automotive industry, NGI has been used mainly as a material in axles and hubs due to its higher ductility and better fatigue properties compared to grey cast iron, often exhibiting properties close to those of steel.

Grey cast iron is generally considered easy to machine with good chip breakability and low cutting forces [Sirtuli 2024]. However, grades such as NGI have proven considerably more challenging to machine, with shorter tool life leading to losses in productivity being one of the main hurdles for the adoption of these cast iron grades [de Sousa 2018]. As such, establishing the reasons for their lower machinability has been thoroughly studied for many years.

Cast irons consist of the metallic matrix with graphite particles of different morphologies. As such, both parts influence the machinability of the material. A study [Fatahalla 1996] found that the machinability of nodular cast iron depended both on the ductility and the amount of graphite nodules in the workpiece material, where a lower ductility and higher amount of graphite nodules yielded worse machinability. An explanation of this was given in [Yang 2024] which showed that the graphite nodules in NGI act as hindrances to stress propagation. Moving on to other cast iron constituents, a study [Nayyar 2012] showed the influence of the matrix composition on cast iron machinability. NGIs with a higher amount of pearlite generally showed inferior machinability as compared to that of ferritic NGIs due to the higher tensile properties of the pearlite in the matrix.

Nevertheless, it is important to recognise that machinability is not solely governed by the mechanical properties of the workpiece material. Rather, it is also significantly influenced by machining method, process parameters, cutting tool characteristics and, as shown in [Malakizadi 2018] and [Lindvall 2023] in the case of CGI milling, the microconstituents of the workpiece material. For example, the geometry of the cutting tool is well known to influence cutting forces, a property often regarded as a major machinability indicator. Moreover, the specific chemical composition and structure of both cemented carbide coatings and substrates is particularly impactful on the performance of tools when machining a given workpiece material. The degradation mechanisms of Ti(C,N)–Al_2O_3 multilayer coating, as studied in [Lindvall 2023], highlighted the complex mechanisms contributing to the wear of coatings when machining CGI. Additionally, the specific properties of the substrate have been shown to be of importance for the wear resistance of coated cemented carbide. As reported in [Garcia 2013], tool life of coated cemented carbides can be enhanced with gradient sintered substrates with a layer of increased hardness close to the coating. Alternatively, the substrate can be modified to have

a layer of reduced hardness and increased toughness close to the coating. This has been shown to improve the fracture resistance of the cutting tool [Yang 2015], an especially beneficial property in intermittent applications, a feature commonly observed in cast iron components.

Although several similarities exist between all cast iron grades, the machinability between different grades can vary greatly [Nayyar 2012]. A general trend for all the presented studies is a focus on CGI, showing a lack of thorough studies on the specific wear of NGI utilising contemporary coated cemented carbide grades. As such, the purpose of the present study is to investigate the wear mechanisms active during moderately interrupted turning of nodular cast iron using two different coated cemented carbide grades. The methodology follows an initial material characterisation to investigate material properties influencing the machining process. This is followed by characterisation of the two cutting tool grades in terms of geometry and substrate composition. Lastly, machining tests under a constant spiral cutting length for several cutting speeds was conducted with subsequent characterisation of the worn tools. The methods aim to create an in-depth understanding of the factors contributing to tool wear from the perspective of both workpiece and cutting tool materials by comparing two slightly different coated cemented carbide cutting tools.

2 EXPERIMENTAL

2.1 Workpiece geometry and material

The investigated workpieces were 200 mm long nodular cast iron tubes with an outer diameter of 200 mm and wall thickness of 25mm. Three grooves were present along the length of the tube with the purpose to introduce intermittency during turning. The workpiece geometry is illustrated in Fig. 1. The specific workpiece material is similar to EN-GJS-600-10 as specified in EN 1563.

2.2 Material characterisation

To understand the interaction between tool and workpiece both the material and tool was studied using advanced material characterisation methods.

To investigate potential variations of material properties within one workpiece, two metallographic samples were cut from one workpiece. Herein, these samples are referred to as sample 1 and 2. The cutting process and locations of the samples are illustrated in Fig. 1, where the metallographically analysed surfaces are indicated by arrows. The samples were mounted in conductive resin and polished to a mirror finish. To reveal the microstructure, the samples were etched using 3% Nital. The graphite particles in the samples were characterised by a combination of light optical microscopy (LOM), specifically with a Zeiss Axioscope 7 with Zen Core 2.7, as well as image processing using a MATLAB script. Graphite nodularity, size, and distribution was determined according to SS-ISO 945-4:2020 where a total area of 13 mm^2 was surveyed on each sample. Graphite particles with a major axis length of less than 10 µm were excluded in compliance with the standard.

The determination of non-metallic inclusion (NMI) type, size and amount in the material was performed with scanning electron microscopy (SEM) and energy-dispersive X-ray spectroscopy (EDS). The chemical composition and distribution of NMIs was analysed with the EDS feature analysis software AztecSteel® in the Oxford Aztec system. For inclusion classification, the default high quality steel scheme was used. The analysis was done on a GEMENI 450 FEG-SEM with an Oxford Ultim Max 100 silicon drift EDS detector at 15kV acceleration voltage and 3nA beam current at a magnification of 500X. Particles with an equivalent circular diameter of less than 1 µm were excluded from the analysis. The total surveyed area was 4.7 mm^2 per sample spread across 120 randomly chosen fields. Examples of inclusions found during the quantitative analysis were also further analysed using EDS area-scans with point spectra as well as imaging using secondary electrons (SE) at 10kV acceleration voltage and 1nA beam current in the same SEM microscope.

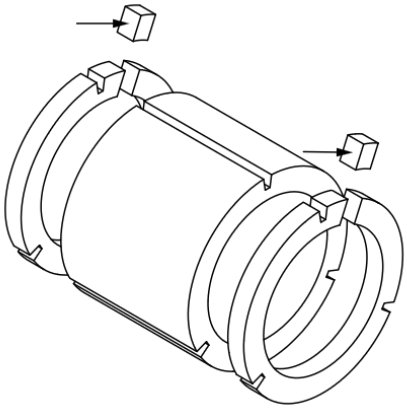

Fig. 1: *Schematic view of workpiece and the location of metallographic samples*

2.3 Cutting tool characterisation

One of the cutting tools were a standard Al_2O_3/TiCN coated grade (herein referred to as grade A), and the other tool was tailored to poses an improved edge toughness while maintaining the nominally similar coating properties (herein referred to as grade B). The two cutting tool grades were characterised by investigation of polished cross sections showing the entire thickness of the inserts close to the cutting edge. The cross sections were examined in the previously mentioned Gemeni SEM with EDS detector both in terms of carbide and binder distribution as well as chemical composition. Additionally, the exact geometry of the rake face could be identified. Lastly, the SEM imaging with EDS and electron backscatter diffraction (EBSD) allowed the tool coatings to be examined in terms of thickness, chemical constituents and texture.

2.4 Machining tests and wear characterisation

The metal cutting tests were performed on an EMCO 365 CNC turning machine equipped with a three-axis dynamometer (Kistler 9257A) under dry condition. Both tested tools were of the same ISO-geometry of CNMG-160616, however differing in terms of chip breaker and rake geometry. The inserts were held by the same PCLNR-2525M-16 holder from Sandvik Coromant resulting in the rake and inclination angles of -6°, and an entering angle of 95°. Four different cutting conditions with varying cutting speeds were tested for both tool grades, seen in Tab. 1. Feed and depth of cut were kept constant at 0.25 mm/rev and 2 mm, respectively. The tested cutting speeds were 275 m/min, 350 m/min, 425 m/min and 500 m/min. This resulted in 16 unique test conditions which all were repeated twice to ensure statistical relevancy.

The test procedure was divided into stints of five face turning passes. After each five passes, the tools were removed from the holder and observed under a stereo optical microscope (SOM) where the flank wear was measured. This process was repeated four times, resulting in a total spiral cutting length (SCL) of 1100 m for each test and its repetition.

Tab. 1: *Tested cutting conditions*

Cutting Speed	Feed	Depth of Cut
275 m/min	0.25 mm/rev	2 mm
350 m/min		
425 m/min		
500 m/min		

When all machining tests were performed, the worn inserts were cleaned using acetone, light brushing and an ultrasonic cleaner. After this, imaging, as well as chemical analysis of adhered material, was performed on a LEO 1550 SEM using SE, backscattered electrons (BSE), and EDS at various magnifications depending on the features of interest.

3 RESULTS

3.1 Material characterisation

From initial investigations in a LOM, the microstructure of the material was observed to mainly consist of ferrite with a small number of pearlite colonies. The pearlite content was approximated to be around 5%. The properties of the graphite present in the two samples are presented in Tab. 2. A relatively large difference in nodularity was seen between the two samples. For sample 1, which had the highest nodularity, the nodule rate is also slightly higher at 44 mm^{-2}. In terms of nodule sizes, both samples show similar results. The overall graphite content was also higher for sample 1 at 12% compared to 10% in sample 2.

Tab. 2: *Graphite properties for the material samples.*

Property	Sample 1	Sample 2
Nodularity	71%	49%
Nodule rate	44 mm^{-2}	41 mm^{-2}
Mean / STD nodule size	101 / 55 µm	101 / 59 µm
Graphite content	12% (Area)	10% (Area)

In terms of non-metallic inclusions, no clear difference could be observed between the two samples. As such, the data from both samples was merged in all following results. The results from the automated NMI analysis are shown in Tab. 3. The inclusions are classified into five types. The group exhibiting largest area fraction were oxides containing magnesium, silicon and calcium. Following that in terms of area fraction were sulphides and nitrides both containing magnesium and silicon. Lastly, with a much smaller area fractions compared to the other groups were carbides containing titanium and niobium and titanium oxides. SEM imaging and elemental maps of two nitrides found in the workpiece material are shown in Fig. 2. The elemental maps were confirmed with point spectra in both inclusions. Similarly, a titanium, niobium carbide is shown in Fig. 3. The average area for oxides, sulphides and nitrides were all around 11 $µm^2$, making the number of observed inclusions the main factor behind differing area fractions. For the titanium containing inclusions both the lower average areas as well as their comparatively low numbers explains their much lower area fractions. A pseudo ternary diagram showing the oxides identified by the NMI software plotted in the CaO-MgO-SiO_2 system is shown in Fig. 4. The diagram also shows the stable phases and liquidus isotherms for the oxide system. Most oxides lie within the MgO region, with some trending towards higher Si content. Little to no oxides containing aluminium were found in the material.

Tab. 3: *Properties of four classes of NMIs found in the workpiece material by automated EDS feature analysis software.*

Constituents	Property	
(Mg,Si,Ca)O	Quantity [-]	1082
	Area Fraction [%]	0. 133
	Mean Area [$µm^2$]	10.8
	Mean Aspect Ratio [-]	1.95
(Mg,Si)S	Quantity [-]	523
	Area Fraction [%]	0. 116
	Mean Area [$µm^2$]	11.6
	Mean Aspect Ratio [-]	1.31
(Mg,Si)N	Quantity [-]	318
	Area Fraction [%]	0.039
	Mean Area [$µm^2$]	11.63
	Mean Aspect Ratio [-]	1.75
(Ti,Nb)C	Quantity [-]	47
	Area Fraction [%]	0.00249
	Mean Area [$µm^2$]	4.99
	Mean Aspect Ratio [-]	2.64
Ti:O	Quantity [-]	26
	Area Fraction [%]	0.00328
	Mean Area [$µm^2$]	11.88
	Mean Aspect Ratio [-]	2.18

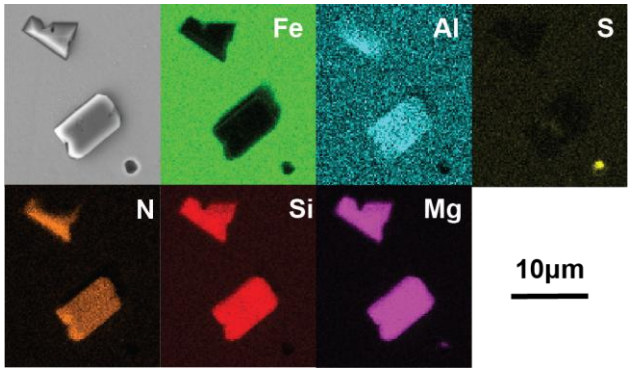

Fig. 2: *Micrograph and EDS elemental maps of (Mg,Si)N inclusion. SE, 10 kV.*

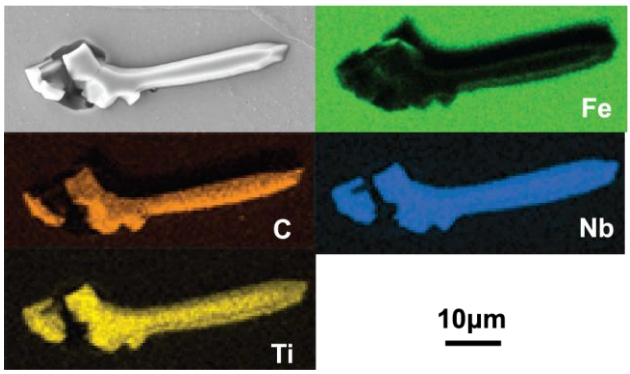

Fig. 3: *Micrograph and EDS elemental maps of (Ti,Nb)C inclusion. SE, 10 kV.*

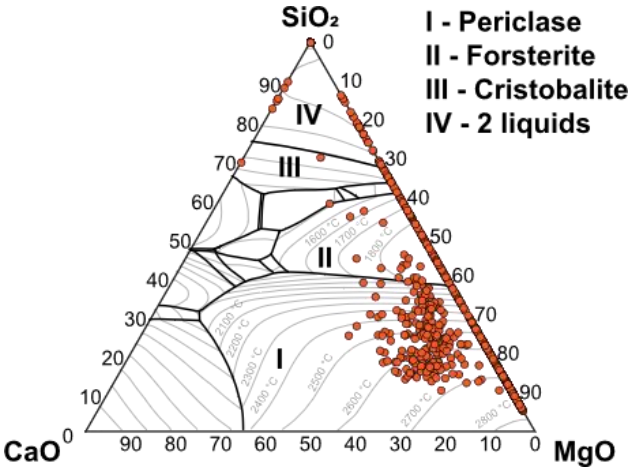

Fig. 4: *Pseudo ternary diagram of the* CaO-MgO-SiO_2 system *showing the composition of oxides in the workpiece material.*

3.2 Tool Characterisation

After investigation of the cutting tool cross sections, several differences were observed between the tools, mainly in the substrate. The coatings on both tools were identified as a multilayer coating with an outer Al_2O_3 layer deposited on a thicker TiCN layer. Based on the EBSD analysis, the Al_2O_3 coating additionally showed indications of being textured along the growth direction in both cases. This was not the case for the TiCN layer in either grade. Further, the substrate of grade A was shown to consist of tungsten carbide (WC) with cobalt binder. Grade B included the same constituents (i.e., WC-Co) with the addition of titanium carbide (TiC), and tantalum/Niobium carbides (TaC/NbC). Additionally, the carbide grain size markedly smaller in grade A, with larger number of smaller carbides dispersed in the substrate. The Tab. 4 summarises findings from the characterisation on the two grades.

Tab. 4: *Properties of the two cutting tool grades.*

Property	Grade A	Grade B
Rake angle*	Neutral	Positive
Coating	Ti(CN)-Al_2O_3	Ti(CN)-Al_2O_3
Substrate	WC-Co	WC-TiC-TaC-Co

* Measured on the rake land before the chip-breaker curvature.

3.3 Metal cutting tests

The measured flank wear during the metal cutting tests can be seen in Fig. 5. The graph lines indicate the average wear measured for both repetitions while the error bars show the actual measurements for both repetitions. It is evident that the flank wear increased with increasing cutting speed for both tool grades. In a similar manner, the wear rate, illustrated by the slope of the wear curves, is noticeably increased with higher cutting speeds. When comparing grade A and grade B across the cutting speeds, grade B shows slightly higher wear overall. Both grades do however exhibit similar wear rates. The difference between repetitions is considered small, and no further repetitions are deemed necessary for improved certainty. Overview SEM images of the inserts exhibiting the largest wear of the two repetitions for both grades at 275 m/min and 550 m/min are seen in Fig. 6. The type of wear is similar for all examples, with differences mainly in the size of the flank wear land and the amount of exposed TiCN coating on the rake face. Minor differences in the amount of adhered material can also be seen. The flank faces of the tools are shown in detail in Fig. 7, clearly showing the brighter exposed TiCN layer closest to the cutting edge followed by the dark Al_2O_3 layer. After the alumina, a small strip of TiCN is remaining. Furthest from the cutting edge is the heat affected zone with a rough surface showing signs of adhered magnesium oxide based on EDS analysis. Randomly spread across the flank faces are even brighter fields of adhered material, shown to be mainly consisting of iron. The chemical compositions for all adhered material have been confirmed with EDS point spectra. Additionally, abrasive marks are indicated by arrows in Fig. 7. The indicated abrasive marks are in this case the clearest examples seen in the SEM imaging. However, many smaller, and less deep marks were also present across the whole flank face of all the observed tools.

The forces measured during the first and last passes of all tests are shown in Fig. 8. The curves show the change in force from the first and last pass of each test. All the curve end points are average values of both repetitions, and the position of the error bar caps denote the actual measured values. When comparing the three measured force directions, the cutting force (F_c) is always the largest by more than double compared to the feed force (F_f) and passive force (F_p). The feed force is similarly also always larger than the passive force by roughly 75 N. The overall forces are the largest for the cutting speeds 275 and 425 m/min. Similarly, increase in measured forces from the first and last pass was largest for these cutting conditions, as seen by the steepest slopes for these conditions. For F_c specifically, the difference between both tool grades is also the most pronounced for these cutting speeds, where grade A clearly produced a higher F_c. In general however, the differences in observed forces between both cutting tool grades and cutting speeds are not distinct, and as such, clear trends are hard to identify. One exception to this is the increase of cutting forces as the tools are worn.

.

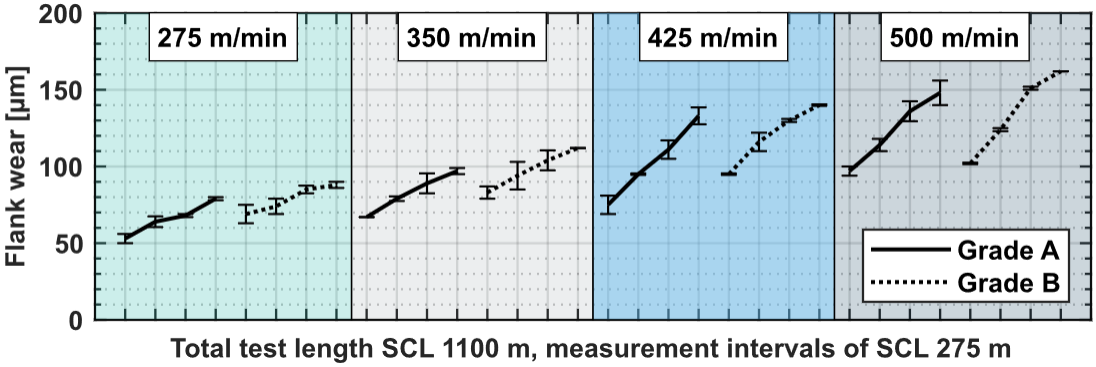

Fig. 5: *Flank wear for both grades across four different cutting conditions.*

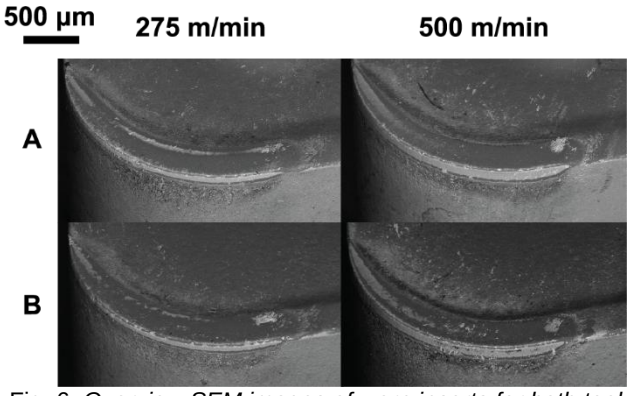

Fig. 6: *Overview SEM images of worn inserts for both tool grades at cutting speeds 275 m/min and 500 m/min.*

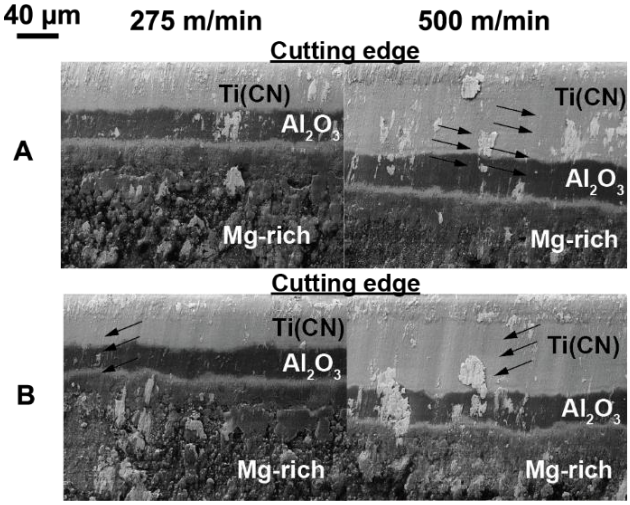

Fig. 7: *Detail SEM images of flank face of worn inserts for both tool grades at cutting speed 275 m/min and 500 m/min. Abrasive marks indicated by black arrows.*

4 DISCUSSION

The discussion aims to connect the results from the metal cutting tests, wear and cutting forces, to the properties of the workpiece and the observed differences in the cutting tool geometry and composition. To begin, the results which were similar for both grades will be discussed.

When it comes to the observed wear. The clearest type during all tested conditions is flank wear. As seen in Fig. 6 and 7 it is, with some exceptions, only on the flank face of the tool that the outer Al_2O_3 layer has been worn away, revealing the brighter TiCN. The fact that the flank wear is even, without chipping or notches, as well as no notable craters being formed on the rake further supports this. When flank wear is the main type of wear, abrasion is often the leading wear mechanism, although combinations of thermo-mechanical, chemical, and adhesive mechanisms often contribute to the progression of this wear type. When looking at the tool flank faces in detail, abrasive marks can be seen (Fig. 7), further supporting the dominance of abrasive wear. For abrasion to take place, abrasive particles should however be present in the material. The (Ti,Nb)C group of inclusions found in the workpiece is such a particle. The wear of a TiCN layer in similarly coated tools when machining CGI was argued to be the result of abrasion from these types of inclusions by [Lindvall 2024] and similarly by [Malakizadi 2018]. The wear of the outer Al_2O_3 layer however, which in the present study accounts for most of the observed wear, an additional mechanism was proposed by Lindvall et.al. The wear of alumina was partly attributed to the adhesion of MgO inclusions on the tool. These particles can react with the Al_2O_3, creating a softer spinel which subsequently would be removed by abrasion. In the present workpiece material, most oxides seem to be of this type, see Fig.4. Additionally, signs of adhered MgO were observed on the worn inserts, particularly in the heat affected zone away from the chip contact zone on both the rake and flank. Since the formation of spinel itself is not what removes the material from the tool, but rather a mechanism of coating degradation, the abrasive marks seen of both layers of the coating is still in agreement with this theory. Further analysis of the tool surfaces as well as cross sections of the worn inserts is needed to with certainty establish the active mechanisms of wear. Based on the findings however, abrasion assisted by adhesion is a likely dominating mechanism.

Moving on to a second similarity. A change in observed forces for different cutting speeds could be seen in a similar manner for both the tested grades. As seen in Fig. 8, especially in the case of F_c, the magnitude is larger for cutting speeds 275 m/min and 500 m/min than for 350 and 425 m/min. The expected trend for the cutting force over cutting speed is either an increase, often due to a higher amount of work hardening from the increased strain rate, or a decrease, often due to thermal softening effects. In the present study, a fluctuation is instead seen. One of the likelier explanations for this is a variation of workpiece properties. As seen in Tab.2 a variation of nodularity was observed within one workpiece. With a difference in nodularity, the mechanical properties of the material and in turn the forces required for cutting can be changed [Fatahalla 1996]. The nodularity has additionally been connected to the cooling rate of the cast, which is known to influence other material properties not directly investigated in the study. Examples of these are the amount of pearlite and the pearlite interlamellar spacing. As such, the conclusion that the nodularity by itself is the reason for the observed differences in cutting forces cannot be made. However, it is likely that some variations of material properties within one workpiece, as well as between different workpieces is behind the variation of forces.

When instead comparing the two cutting tool grades, differences can be seen between the two grades both in terms of wear and cutting forces. In terms of wear, grade B exhibits slightly higher wear, as seen in Fig. 5. The largest difference between the tools were found in the substrate, as seen in Tab.4. The exact implications the observed differences have on the mechanical properties of the substrate has not been investigated in this study. It is however known that a smaller grain size yields a higher hardness, as in grade A, although in a similar manner, the strength of the substrate can be improved with the addition of TiC and TaC, as in grade B. As such, without further study it is not possible to attribute any observed difference in wear to a property of the cutting tool substrate. Additionally, the wear has not yet progressed beyond the coatings, and the currently tested cutting conditions are likely not harsh enough to where the mechanical strength of the substrate will have a major impact on the insert's resistance to plastic deformation. As such, larger differences in wear could potentially be seen if similar tests were performed with much increased depth of cut and feed. Additionally, the preliminary analysis of the coatings showed no significant differences between the two grades. But the specific grain size and texture in the coatings of the observed grades could potentially be the reason for the slightly differing wear seen in this study.

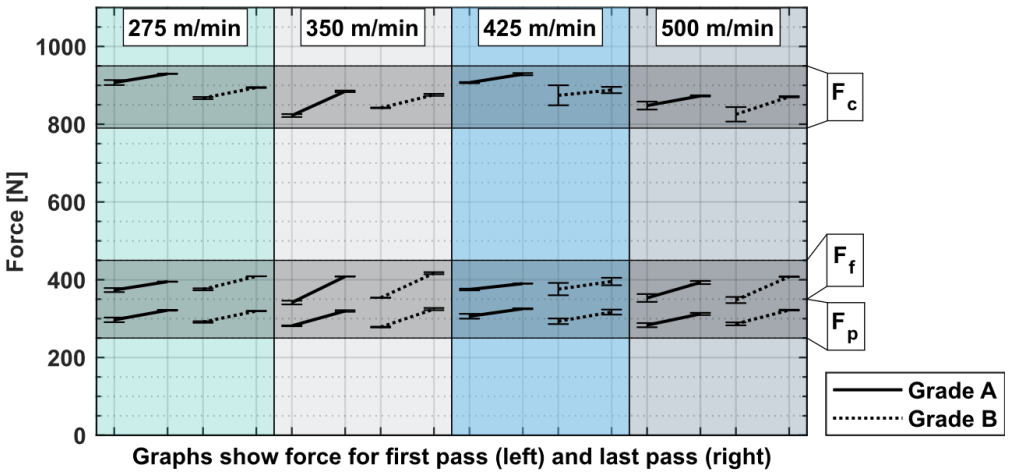

Fig. 8: *Cutting forces measured during the beginning and end of all tests.*

When comparing the two grades in terms of measured cutting forces, as seen in Fig. 8, several differences can be observed. Especially in the case of the cutting force Fc, a trend towards lower forces for grade B can be seen for most cases. A potential explanation for this is the slightly positive rake land found on this grade as compared to the neutral rake on grade A. The angle of the rake will directly impact the observed forces, where a larger negative angle will be generating larger forces. This effect is however overlapping with the previously mentioned differences in material properties across workpieces, making it difficult to with certainty attribute the force difference to the different rake angles of the two inserts.

Based on the findings of the present study, both tested coated cemented carbide grades show industrial applicability for the tested cutting conditions. The wear behaviour is remaining in a range of progressive flank wear without any observed stochastic wear behaviours.

5 CONCLUSIONS

Two different similarly coated cemented carbide tool grades were characterised and used to machine nodular cast iron workpieces. The characterisation of the tools in combination with characterisation of the material and the results from the metal cutting tests made it possible to draw some conclusions about the performance of the two tool grades and the active mechanisms of wear.

- Both studied tool grades show good resistance to wear, showing industrially applicable tool-life for the tested range of cutting conditions.
- The cutting tools showed differences both in terms of rake geometry and substrate microstructure and chemical composition, the impacts of which on tool wear behaviour were not significant within the range of cutting conditions in this investigation.
- Abrasion supported by adhesion seems to be the leading wear mechanism for both tools at all tested cutting conditions. This is supported by the presence of inclusions in the material that are known to act abrasively as well as to decompose the Al_2O_3 coating.

6 ACKNOWLEDGEMENTS

This study was part of the WEAR-FRAME project funded by Vinnova (Sweden's Innovation Agency) under FFI program (Project No.2020- 05179). The supports received from the Chalmers Area of Advance – Production and the Chalmers Centre for Metal Cutting Research (MCR) are acknowledged. The authors would also like to extend their gratitude to Jonas Svensson from Volvo Group for the valuable discussions and input.

7 REFERENCES

[de Sousa 2018] de Sousa, J.A.G et.al. A review on the machining of cast irons. The International Journal of Advanced Manufacturing Technology, September 2018, Vol. 94, pp 4073–4092.

[Fatahalla 1996] Fatahalla, N. et.al. Metallurgical parameters, mechanical properties and machinability of ductile cast iron. Journal of Materials Science, November 1996, Vol.31, No.21, pp 5765-5772. ISSN 1573-4803.

[Garcia 2013] Garcia, J and Pitonak, R. The role of cemented carbide functionally graded outer-layers on the wear performance of coated cutting tools. International Journal of Refractory Metals and Hard Materials, January 2013, Vol.36, pp 52-59. ISSN 0263-4368.

[Górny 2015] Górny, M. Microstructure and Properties of Ductile Iron and Compacted Graphite Iron Castings. Cham: Springer International Publishing 2015. ISBN 978-3-319-14583-9.

[Lindvall 2023] Lindvall, R. et.al. Degradation of multi-layer CVD-coated cemented carbide in finish milling compacted graphite iron. Wear, June 2023, Vol.522, 204724. ISSN 0043-1648.

[Malakizadi 2018] Malakizadi, A. et.al. Effects of workpiece microstructure, mechanical properties and machining conditions on tool wear when milling compacted graphite iron. Wear, July 2018, Vol.410-411, pp 190-201. ISSN 0043-1648.

[Nayyar 2012] Nayyar, V. et.al. An Experimental Investigation of Machinability of Graphitic Cast Iron Grades; Flake, Compacted and Spheroidal Graphite Iron in Continuous Machining Operations. Procedia CIRP, 2012, Vol.1, pp 488-493. ISSN 2212-8271.

[Sirtuli 2024] Sirtuli, L. J. et.al. Machining of Compacted Graphite Iron: A review. Journal of Materials Processing Technology, November 2024, Vol.332, 118553. ISSN 0924-0136.

[Yang 2024] Yang, H. W. et.al. Influence of distribution and size of graphite particle on the machinability of nodular cast iron. Engineering Fracture Mechanics, February 2024, Vol.297, 109882. ISSN 0013-7944.

[Yang 2015] Yang, TE. et.al. Adherent coating on gradient cemented carbide with ultrafine Ti(C0.5,N0.5). Rare metals, January 2015, Vol.34, No.6, pp 413–420. ISSN 1867-7185.